Identification and modulation of electronic band structures of single-phase β-$(Al_xGa_{1-x})_2O_3$ alloys grown by laser molecular beam epitaxy

Jing Li, Xuanhu Chen, Tongchuan Ma, Xiangyuan Cui, Fang-Fang Ren, Shulin Gu, Rong Zhang, Youdou Zheng, Simon P. Ringer, Lan Fu, Hark Hoe Tan, Chennupati Jagadish, and Jiandong Ye

Citation: Appl. Phys. Lett. **113**, 041901 (2018); doi: 10.1063/1.5027763
View online: https://doi.org/10.1063/1.5027763
View Table of Contents: http://aip.scitation.org/toc/apl/113/4
Published by the American Institute of Physics

Articles you may be interested in

Donors and deep acceptors in β-Ga_2O_3
Applied Physics Letters **113**, 062101 (2018); 10.1063/1.5034474

Demonstration of high mobility and quantum transport in modulation-doped β-$(Al_xGa_{1-x})_2O_3$/Ga_2O_3 heterostructures
Applied Physics Letters **112**, 173502 (2018); 10.1063/1.5025704

Optical signatures of deep level defects in Ga_2O_3
Applied Physics Letters **112**, 242102 (2018); 10.1063/1.5026770

Band alignment of In_2O_3/β-Ga_2O_3 interface determined by X-ray photoelectron spectroscopy
Applied Physics Letters **113**, 031603 (2018); 10.1063/1.5038615

Energy band engineering of InGaN/GaN multi-quantum-well solar cells via AlGaN electron- and hole-blocking layers
Applied Physics Letters **113**, 043501 (2018); 10.1063/1.5028530

Structural and electronic properties of Ga_2O_3-Al_2O_3 alloys
Applied Physics Letters **112**, 242101 (2018); 10.1063/1.5036991

Identification and modulation of electronic band structures of single-phase β-$(Al_xGa_{1-x})_2O_3$ alloys grown by laser molecular beam epitaxy

Jing Li,[1] Xuanhu Chen,[1] Tongchuan Ma,[1] Xiangyuan Cui,[2,a)] Fang-Fang Ren,[1,3,4] Shulin Gu,[1,4] Rong Zhang,[1,4] Youdou Zheng,[1,4] Simon P. Ringer,[2] Lan Fu,[3] Hark Hoe Tan,[3] Chennupati Jagadish,[3] and Jiandong Ye[1,3,4,a)]

[1]*School of Electronic Science and Engineering, Nanjing University, Nanjing 210093, China*
[2]*Australian Centre for Microscopy and Microanalysis and School of Aerospace, Mechanical and Mechatronic Engineering, The University of Sydney, Sydney, New South Wales 2006, Australia*
[3]*Department of Electronic Materials Engineering, Research School of Physics and Engineering, The Australian National University, Canberra, Australian Capital Territory 2601, Australia*
[4]*Collaborative Innovation Center of Solid-State Lighting and Energy-Saving Electronics, Nanjing University, Nanjing 210093, China*

(Received 5 March 2018; accepted 6 July 2018; published online 23 July 2018)

Understanding the band structure evolution of $(Al_xGa_{1-x})_2O_3$ alloys is of fundamental importance for developing Ga_2O_3-based power electronic devices and vacuum ultraviolet super-radiation hard detectors. Here, we report on the bandgap engineering of β-$(Al_xGa_{1-x})_2O_3$ thin films and the identification of compositionally dependent electronic band structures by a combination of absorption spectra analyses and density functional theory calculations. Single-monoclinic β-phase $(Al_xGa_{1-x})_2O_3$ ($0 \le x \le 0.54$) films with a preferred (−201) orientation were grown by laser molecular beam epitaxy with tunable bandgap ranging from 4.5 to 5.5 eV. The excellent fitting of absorption spectra by the relation of $(\alpha h\nu)^{1/2} \propto (h\nu\text{-}E)$ unambiguously identifies that β-$(Al_xGa_{1-x})_2O_3$ alloys are indirect bandgap semiconductors. Theoretical calculations predict that the indirect nature of β-$(Al_xGa_{1-x})_2O_3$ becomes more pronounced with increased Al composition due to the increased eigenvalue energy gap between M and Γ points in the valence band. The experimentally determined indirect bandgap exhibits almost a linear relationship with Al composition, which is consistent with the theoretical calculation and indicates a small bowing effect and a good miscibility. The identification and modulation of $(Al_xGa_{1-x})_2O_3$ band structures allows rational design of ultra-wide bandgap oxide heterostructures for the applications in power electronics and solar-blind or X-ray detection. *Published by AIP Publishing.* https://doi.org/10.1063/1.5027763

Gallium oxide (Ga_2O_3) is an emerging candidate for the applications of solar blind photodetectors, high power transistors due to its ultra-large band gap of 4.8 eV, high breakdown field, high electron saturation velocity, and high hardness irradiation.[1–5] To further exploit the potential of Ga_2O_3 material, bandgap engineering of $(Al_xGa_{1-x})_2O_3$ and heterostructure designs are on demand. Bandgap tunability of $(Al_xGa_{1-x})_2O_3$ alloying up to above 6 eV enables to develop vacuum ultraviolet (VUV) super-radiation hard detectors.[6] Furthermore, $(Al_xGa_{1-x})_2O_3/Ga_2O_3$ based high electron mobility transistors (HEMTs) with a two-dimensional electron gas channel has been demonstrated through Si delta-modulation doping.[7–9] Whereas the channel mobility is still not far enough for high frequency applications, as it is limited by polar optical phonon scattering due to a higher electron effective mass of 2DEG.[7] The device performance of photodetectors and transistors are normally determined by the optical transition nature and intrinsic effective mass, and therefore, a deep understanding of the fundamental properties of $(Al_xGa_{1-x})_2O_3$ alloying materials is critical. Despite a handful of reports on the bandgap modulation of $(Al_xGa_{1-x})_2O_3$ and demonstrations of modulation-doped HEMT, the experimentally obtained bandgap values exhibit a strong dependence on the synthesis methods and growth conditions.[10,11] In particular, most reports treated β-Ga_2O_3 and $(Al_xGa_{1-x})_2O_3$ as direct bandgap materials while no band emission with direct transition has been observed. These contradictory facts are also inconsistent with the theoretical predictions of the electronic band structure of β-Ga_2O_3.[12,13] The effects of intrinsic defects on the electronic and optical properties of β-Ga_2O_3 doped by a small composition of Al has been investigated with first-principles calculation, whereas the electronic band structural evolution of $(Al_xGa_{1-x})_2O_3$ with a full compositional range of Al and the nature of optical transitions are still not well understood.[14] Here, wide bandgap engineering of composition tunable single-monoclinic β phase $(Al_xGa_{1-x})_2O_3$ ($0 \le x \le 0.54$) thin films were achieved through laser molecular beam epitaxy (LMBE) technique. The evolution of structural phase and indirect optical transition of the alloying films were identified using absorption spectra analyses in combination with first principles simulation. The correlation of the optical transition with the electronic band structure is discussed in detail.

$(Al_xGa_{1-x})_2O_3$ alloying films were grown on single polished (0001) sapphire by LMBE using a various $(Al_xGa_{1-x})_2O_3$ targets which were sintered by mixing high purity (99.999%) Ga_2O_3 and Al_2O_3 powders with precisely controlled mole ratio, as shown in Table I. Before growth, the sapphire substrates were chemically etched in hot

a)Authors to whom correspondence should be addressed: carl.cui@sydney.edu.au and yejd@nju.edu.cn

(60 °C) H_2SO_4 (98%), ultrasonically cleaned in ethanol and acetone, rinsed in deionized water, and blow-dried with nitrogen flow. The distance between targets and substrates were maintained at 7 cm. A 248 KrF excimer laser with a pulse repetition of 1 Hz and a pulse energy of 225 mJ was used to ablate the target. The base pressure of the growth chamber was evacuated below 2×10^{-8} Torr. According to the optimized growth window for β-Ga_2O_3 material, the partial pressure of oxygen ambient (99.999%) was fixed at 5×10^{-3} Torr, and the substrate temperature was maintained at 800 or 850 °C. The microstructures of $(Al_xGa_{1-x})_2O_3$ were characterized by high resolution X-ray diffraction (HRXRD) using a D8 advance system with a Cu Kα X-ray source and angle reproducibility of ±0.0001°. X-ray photoelectron spectra were recorded by a ULVAC-PHI 5000 versa probe system with an Al Kα X-ray source. Optical transmission spectra were recorded by a UV-visible near-IR scanning spectrophotometer (Lambda 950, PerkinElmer). To identify the structural and electronic structure evolution of $(Al_xGa_{1-x})_2O_3$, density functional theory (DFT) calculations with the generalized gradient approximation (GGA) of Perdew, Burke, and Ernzerhof and the screened hybrid functional of Heyd, Scuseria, and Ernzerhof (HSE), as implemented in the VASP code were conducted.[15–17] In the HSE calculations, the Hartree-Fock mixing parameter was set to 0.3. The plane wave basis set cutoff energy of 500 eV was used. The energy convergence criterion between two electronic steps was 10^{-4} eV. The first Brillouin zone was sampled by a *k*-mesh of $(6 \times 24 \times 12)$ and $(12 \times 12 \times 4)$ for the β- and α-Ga_2O_3, respectively. Atomic positions were optimized in all the calculations until the maximum force on each atom is less than 0.02 eV/Å.

The Al contents in the $(Al_xGa_{1-x})_2O_3$ samples, where x ranges from 0 to 0.54, were determined from the results of XPS analyses (XPS spectra are shown in Fig. S1). Figure 1(a) shows the HRXRD patterns of 2θ-ω scans of the alloy films in the logarithmic scale. Among all the measured samples, no peak corresponding to phases other than β-$(Al_xGa_{1-x})_2O_3$ or sapphire substrate was detected, showing that the films are of pure monoclinic β phase. Three dominant diffraction peaks located around 19.1°, 38.4°, and 60.3° were observed for the films with low Al composition ($x < 0.3$), which are assigned as the (−2 0 1), (−4 0 2), and (−6 0 3) planes, respectively. The XRD intensity markedly decreases for the samples with the higher inclusion levels of Al. It is noticed that (−2 0 1) diffraction peaks are almost absent while the diffraction peaks of (−6 0 3) and (−8 0 4) are still dominant in the XRD patterns of β-$(Al_xGa_{1-x})_2O_3$ ($x > 0.3$) films. It can be understood that the low indexed reflex (−2 0 1) with a small incident angle suffer from more serious incoherent scattering for the smaller lateral grain sizes due to the crystalline degradation. Similar phenomena have also been observed in the hetero-epitaxial growth of $(Al_xGa_{1-x})_2O_3$ on sapphire by various means of MBE, pulsed laser deposition (PLD), and, MIST-CVD techniques.[10,18,19] The reported phase transition from a stable pseudomorphic α-$(Al_xGa_{1-x})_2O_3$ ultra-thin interfacial layer into a plastically relaxed and textured monoclinic β-$(Al_xGa_{1-x})_2O_3$ in the form of rotational domains is also observed, as shown in supplementary material, Fig. S2.[20] The crystalline degradation is attributable to the relatively low growth temperature for crystallization of β-$(Al_xGa_{1-x})_2O_3$ as it is optimized for pure β-Ga_2O_3.[10,18,19] Nevertheless, the dominant (−6 0 3) diffraction peaks indicate the grown films are of the single phase with a preferred (−2 0 1) orientation. Figure 1(b) exhibits that the position of the (−6 0 3) peaks shows a monotonic shift to the higher angle side, which suggests a shrinking in the lattice constant of (−2 0 1) due to the smaller ionic radius of the Al^{3+} ions substituting Ga^{3+} ions. According to Kranert's report, a group of equations on the relationship between Al content x and lattice parameter based on Vegard's law are $a = (12.21 - 0.42x)$Å, $b = (3.04 - 0.13x)$Å, $c = (5.81 - 0.17x)$Å, and $\beta = (103.87 + 0.31x)°$.[21] Considering the monoclinic structure, the plane space of (−6 0 3) can be expressed as $d = \left(\frac{h^2}{a^2\sin^2\beta} + \frac{l^2}{c^2\sin^2\beta} - \frac{2hl\cos\beta}{ac\sin^2\beta} + \frac{k^2}{b^2}\right)^{-\frac{1}{2}}$, where h = −6, k = 0, and l = 3. As a consequence, the Al content, x can be determined from the positions of (−6 0 3) diffraction peaks. As shown in Fig. 2(a), the composition of Al calculated from XRD patterns by the above equations agrees very well with the values determined by XPS measurements shown in Table I. It strongly suggests that most of the Al atoms have been incorporated in the alloy lattice, i.e., β-$(Al_xGa_{1-x})_2O_3$ system has a good miscibility.[22]

To investigate the substitutional behavior of Al in β-$(Al_xGa_{1-x})_2O_3$, the system stability with different Al concentrations (i.e., various numbers of Al atoms, ranging from

TABLE I. List of $(Al_xGa_{1-x})_2O_3$ samples investigated including measured XPS composition, target composition, substrate temperatures, and film thickness determined by transmittance spectra.

Sample	XPS composition x =	Target Al_2O_3 at. %	Substrate temperature (°C)	Thickness (nm)
A	0.32	30 (commercial)	800	479
B	0.54	50 (commercial)	800	341
C	0.17	10 (home made)	850	267
D	0.30	20 (home made)	850	253
E	0.34	30 (home made)	850	204
F	0.42	40 (home made)	850	172
Reference	0	0 (commercial)	800	525

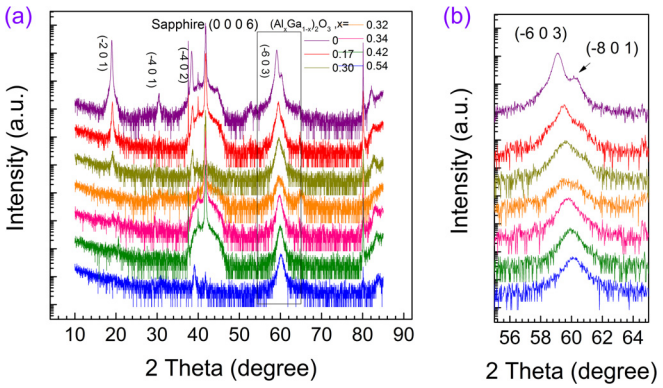

FIG. 1. (a) HRXRD 2θ-ω spectra of $(Al_xGa_{1-x})_2O_3$ films; (b) an enlarged plot for (−6 0 3) planes of $(Al_xGa_{1-x})_2O_3$.

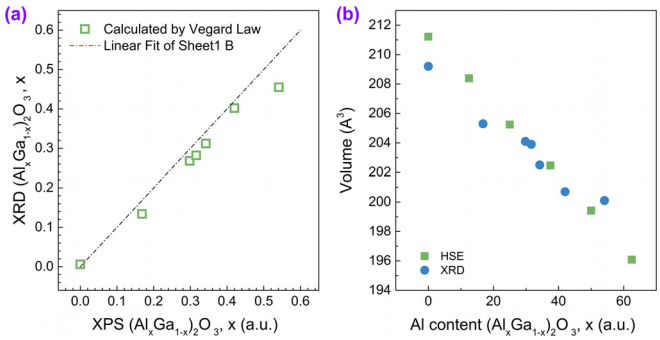

FIG. 2. (a) Comparison between composition determined by XPS and XRD; (b) comparison between cell volumes calculated from XRD and HSE simulation.

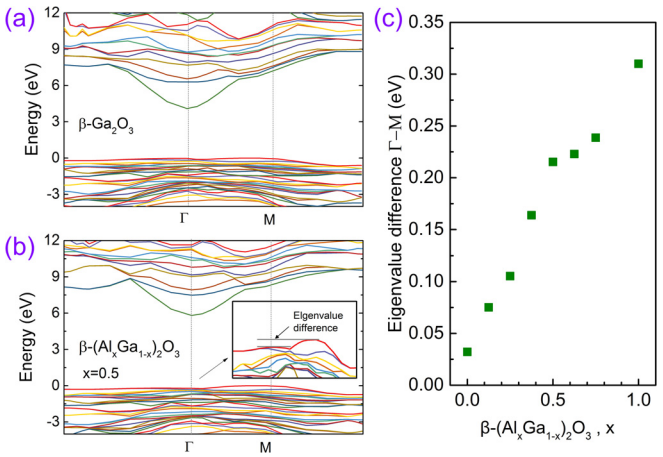

FIG. 3. Electronic band structure of β-$(Al_xGa_{1-x})_2O_3$ obtained from HSE calculations for (a) $x = 0$ and (b) $x = 0.5$; (c) VBM eigenvalue differences between the M and Γ points as a function of Al concentration.

0 to 6) to substitute Ga atoms in β-Ga_2O_3 unit cell were simulated in the DFT framework. For each alloy, several initial atomic configurations have been considered, where the calculated energetically favorable structures are shown in Fig. S3. It is found that Al ions prefer to substitute Ga tetrahedral sites in fully relaxed atomic structures. This preference can be explained as the consequence of the fact that Al^{3+} has smaller ionic radius than that of Ga^{3+} with lower formation energy.[23] A good consistency between experimental cell volume, deduced from XRD, and the fully relaxed theoretical DFT-HSE results was obtained, as exhibited in Fig. 2(b), despite a small deviation observed for low Al compositions. This indicates the validity of the setup of atomic configuration in DFT calculation, which is important for the accurate prediction of electronic band structures. Note that experimentally, the $(Al_xGa_{1-x})_2O_3$ layer may still be partially strained to the sapphire substrate, consistent with the strain analysis of $(Al_xGa_{1-x})_2O_3/Al_2O_3$ interface by the high-resolution cross-section transmission electron microscopy (Fig. S2), which results in the cell volume deviating from that of the fully relaxed structure, particularly more so for samples with lower Al content.

On the aspect of electronic band structure of β-$(Al_xGa_{1-x})_2O_3$, both GGA and HSE calculations were performed in terms of first principles, which has been widely employed to predict a variety of electronic, optical, and magnetic properties of polycrystalline oxide semiconductors.[24–28] The specific electronic band structures of the alloy films with composition of $x = 0$ and $x = 0.5$ are shown in Figs. 3(a) and 3(b), respectively. It is found that the valence band maximum (VBM) locates at the M point (½, ½, ½), which is only 0.032 eV (0.070 eV) higher than Γ (0, 0, 0) as calculated by HSE (GGA), which strongly suggests that β-Ga_2O_3 is an indirect bandgap semiconductor, in agreement with previous theoretical studies.[12,13] Notably, the indirect nature of optical transition is retained after alloying with Al, and the VBM eigenvalue differences between the M and Γ points become larger as the Al content increases in β-$(Al_xGa_{1-x})_2O_3$, as shown in Fig. 3(c). The indirect bandgap nature of β-$(Al_xGa_{1-x})_2O_3$ is as expected when one considers the fact that the top valence band is predominantly formed by O-2p orbitals. Indeed, our preliminary DFT results suggest that cation alloying (by Al-, In-, or by both) does not change the indirect nature of the band structure. In general, if materials are direct wide-bandgap semiconductors, band-to-band emissions would be observed in much stronger intensity than the defective emissions. In fact, on the emission properties of β-Ga_2O_3 by both photoluminescence and cathodoluminescence, only defect emissions such as broad blue and ultraviolet emission peak near 2.9 eV and 3.3 eV, respectively, have been widely reported, while the optical emission directly from conduction band to valence band has yet to be reported.[29–31] The absence of near-band edge emission is an indication of the indirect nature of electronic band structure of β-Ga_2O_3 materials. Residual strain may affect the electronic band structure, especially for the layer in the vicinity of the substrate. Based on electronic diffraction patterns (Fig. S2), the residual strain in the sample of $x = 0.17$ was estimated to be less than 1.2%. According to our theoretical calculations performed on β-$(Al_xGa_{1-x})_2O_3$ with $x = 0$, 0.125, 0.25, 0.375, and 0.50, biaxial 1.5% tensile strain on the a-b plane tends to reduce the bandgap values by 0.10 eV–0.15 eV, yet the indirect bandgap nature remains (Table S2). Meanwhile, the calculated electron effective mass values for $(Al_xGa_{1-x})_2O_3$ were found to increase by adding Al—ranging from 0.265 m_e for $x = 0$, to 0.376 m_e for $x = 0.5$ and finally to 0.437 m_e for $x = 1$. For β-Ga_2O_3, similar values were reported, both theoretically[13,32] and experimentally (0.28 m_e).[33] Recently, the effective mass of the 2DEG formed at $(Al_xGa_{1-x})_2O_3/Ga_2O_3$ ($x = 0.2$) interface is estimated to be 0.313 m_e,[7] which is related to the strong electron-electron interaction.[34]

The electronic band structure and bandgap modulation by Al incorporation can also be evaluated by absorption spectra. Transmittance spectra of β-$(Al_xGa_{1-x})_2O_3$ film samples have been recorded at room temperature and shown in Fig. S4. The observed oscillation features below the bandgap are attributed to the interference effect between the topmost surface of $(Al_xGa_{1-x})_2O_3$ and $(Al_xGa_{1-x})_2O_3/Al_2O_3$ interface, from which the thickness of samples can be determined. Generally, the growth rate decreases with the increasing of Al content in the range of 172–479 nm, as shown in Table I. As a result of bandgap modulation, steep absorption edges exhibit a monotonous shift from the wavelength of 250 to 200 nm as Al content increases from 0 to 0.54. The absorption coefficient (α) can then be obtained

from $\exp(-\alpha d) = T/(1-R)$ (d is the film thickness, T is the transmittance, and R is the reflectance).[35] Typically, the optical bandgap can be evaluated by using the well-known Tauc rules of $(\alpha h\nu)^n = A(h\nu - E_g)$, where the value of the exponent, n, denotes the nature of the optical transitions.[36] Good linearity of $(\alpha h\nu)^n$ versus $h\nu$ is expected when n equals 1/2 for indirect allowed transition or n equals 2 for direct bandgap. Figures 4(a) and 4(b) show the $(\alpha h\nu)^{1/2}$ and $(\alpha h\nu)^2$ curves as a function of photon energy, $h\nu$ for all samples derived from the original transmittance spectra in Fig. S4. It is clear that plots of $(\alpha h\nu)^{1/2}$ versus $h\nu$ exhibits a much better linearity relationship than that of $(\alpha h\nu)^2$ versus $h\nu$. The detailed linear analyses on the absorption spectra are shown in Fig. S4, which confirmed that n = 1/2 curve has a better linearity with smaller deviation error. The above analysis unambiguously identified the indirect band structure of β-$(Al_xGa_{1-x})_2O_3$, in good agreement with the theoretical calculation results discussed earlier.

The indirect bandgap values are determined from the linear extrapolation of $(\alpha h\nu)^{1/2}$ versus $h\nu$ curves in Fig. 4(a) and summarized in Fig. 5. In this work, tunable indirect bandgap has been achieved from 4.5 to 5.5 eV, corresponding to the Al content x from 0 to 0.54, respectively. For a better comparative study, the fitting results of $(\alpha h\nu)^2$ versus $h\nu$ curves were also plotted in Fig. 4(b) and summarized in the form of scatter plot in Fig. 5, together with the data of β-$(Al_xGa_{1-x})_2O_3$ synthesized via PLD and solution combustion synthesis from literatures.[10,11] To distinguish the data, spot groups denoted as "D" are the direct bandgap derived from linear fitting of $(\alpha h\nu)^2$ curves. Likewise "ID" denotes

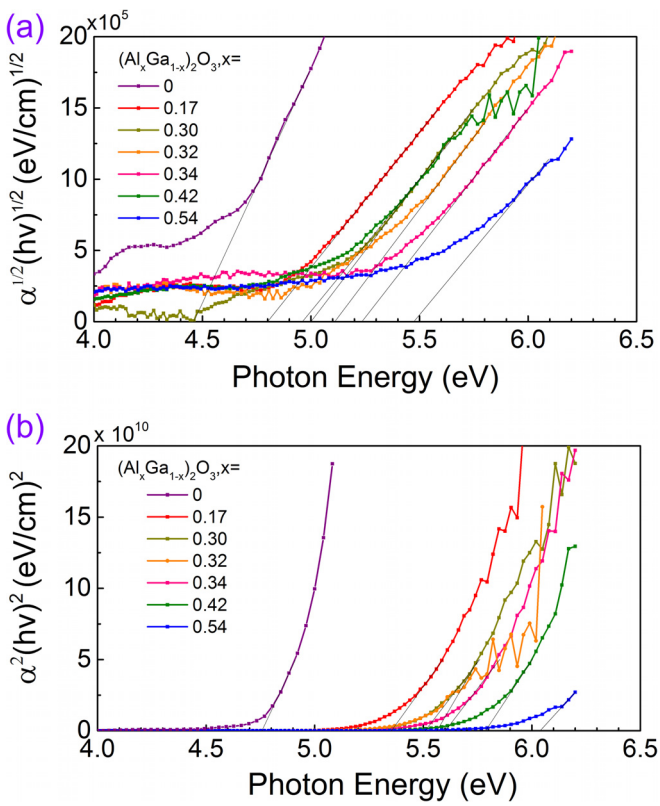

FIG. 4. Spectra of (a) $(\alpha h\nu)^{1/2}$ and (b) $(\alpha h\nu)^2$ calculated from the transmission spectra of the β-$(Al_xGa_{1-x})_2O_3$ samples after subtraction of the contribution from sapphire substrate.

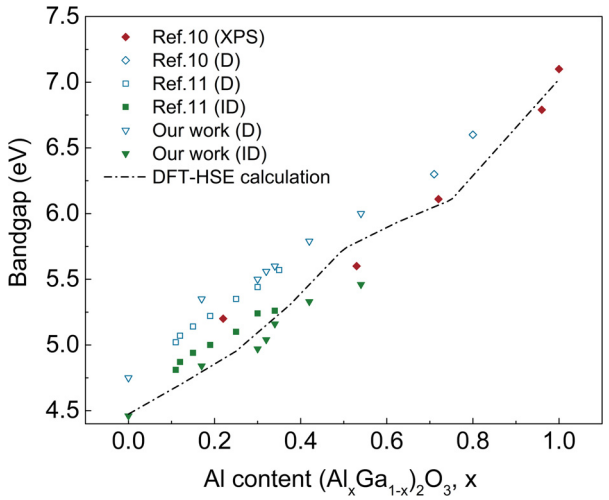

FIG. 5. Bandgap versus composition of β-$(Al_xGa_{1-x})_2O_3$ plots obtained from our experiment and HSE simulation, and recent experimental studies. Reproduced with permission from Appl. Phys. Lett. **105**, 162107 (2014). Copyright 2014 AIP Publishing LLC[10] and reproduced with permission from J. Appl. Phys. **117**, 165307 (2015). Copyright 2015 AIP Publishing LLC.[11]

the indirect bandgap data obtained linear fitting of the $(\alpha h\nu)^{1/2}$ curves. The bandgap values show consistency with reported data and good linearity with increasing Al content. Spot groups marked as "XPS" were obtained by measuring electronic energy loss extracted from XPS, which is closer in agreement with the indirect bandgap "ID" group than the direct bandgap "D" group. Furthermore, a good agreement between the DFT calculation and data from the "ID" group confirms the indirect nature of the band structure. In general, the compositional dependence of the bandgap of β-$(Al_xGa_{1-x})_2O_3$ can be described with a bowing effect[28]

$$E_g^{AlGaO} = xE_g^{GaO} + (1-x)E_g^{AlO} + C_g(1-x)x,$$

where E_g^{GaO}, E_g^{AlO}, and E_g^{AlGaO} denote the bandgap value of the Ga_2O_3, Al_2O_3, and their alloy, respectively, and C_g is the bowing parameter. Here, the bowing parameter for indirect bandgap was calculated to be −1.3. In the case of $(Al_xGa_{1-x})_2O_3$, small values of the bowing parameter are observed in α-, β-, and γ-$(Al_xGa_{1-x})_2O_3$.[10,19,21,28] Typically, a small value of the bowing parameter and thus a small deviation from the linearity of the bandgap of alloys can indicate a desirable miscibility,[37] which is in agreement with the XRD results. The bandgap of 4.5–5.5 eV is corresponding to the absorption wavelength between 225 nm and 275 nm in the solar blind spectral range.[6,38,39] After post-annealing with 1500 °C for 4 h, due to intensive solid reaction and inter-diffusion between the Al_2O_3 substrate and β-$(Al_xGa_{1-x})_2O_3$ layer, composition-gradient β-$(Al_xGa_{1-x})_2O_3$ film was formed with a bandgap of 6.2 eV (calculated via XPS electronic energy loss). In this case, the wavelength of absorption cut-off edge could be extended to 200 nm, reaching the spectral range of vacuum ultraviolet. Considering the inherent advantage of β-$(Al_xGa_{1-x})_2O_3$ on resistance to radiation damage and chemical stability, β-$(Al_xGa_{1-x})_2O_3$ shows promising applications in solar blind and VUV superradiation hard detector for space objects.

In summary, bandgap tuning of monoclinic single-phase β-$(Al_xGa_{1-x})_2O_3$ $(0 \le x \le 0.54)$ thin films with preferred

(−2 0 1) orientations were achieved through LMBE technique. The lattice variation induced by Al composition follows Vegard's law, in agreement with the calculated results of fully relaxed structures in the DFT framework. The consistency of experimental data and calculated electronic band structure strongly suggests that β-$(Al_xGa_{1-x})_2O_3$ has an indirect nature of optical transitions with an ineligible eigenvalue differences between the M and Γ points and the effective electron mass values increase as Al composition increases. A small bowing effect for compositional dependence of bandgap of β-$(Al_xGa_{1-x})_2O_3$ indicates excellent miscibility due to the preference of Al substituting the Ga tetrahedral sites. The bandgap tunability of β-$(Al_xGa_{1-x})_2O_3$ and the understanding on the band structure evolution allow one to design wide-gap oxide heterostructures with desirable wavelength response for the future applications in high frequency and high power electronics, solar-blind photodetection, and high-energy ray detection.

See supplementary material for (1) XPS data and composition determination of β-$(Al_xGa_{1-x})_2O_3$ film samples; (2) cross-section transmission electron microscopy; (3) the crystal structure evolution of β-$(Al_xGa_{1-x})_2O_3$; (4) the influence of strain on electronic structure; (5) transmittance spectra of β-$(Al_xGa_{1-x})_2O_3$ film samples; and (6) linearity analysis on absorption spectra.

This research was supported by the National Key Research and Development Project (Grant No. 2017YFB0403003), the National Natural Science Foundation of China (Grant Nos. 61774081, 61322403, and 11227904), the Natural Science Foundation of Jiangsu Province (Grant Nos. BK20130013 and BK20161401), the Six Talent Peaks Project in Jiangsu Province (2014XXRJ001), the Fundamental Research Funds for the Central Universities (021014380093 and 021014380085) and the Australian Research Council. The computational part of this research was undertaken with the assistance of resources from the National Computational Infrastructure (NCI), which is supported by the Australian Government under the NCRIS program.

[1]M. Higashiwaki, K. Sasaki, H. Murakami, Y. Kumagai, A. Koukitu, A. Kuramata, T. Masui, and S. Yamakoshi, Semicond. Sci. Technol. **31**, 034001 (2016).
[2]M. Higashiwaki, K. Sasaki, T. Kamimura, M. H. Wong, D. Krishnamurthy, A. Kuramata, T. Masui, and S. Yamakoshi, Appl. Phys. Lett. **103**, 123511 (2013).
[3]A. J. Green, K. D. Chabak, M. Baldini, N. Moser, R. C. Gilbert, R. Fitch, G. Wagner, Z. Galazka, J. Mccandless, A. Crespo, K. Leedy, and G. H. Jessen, IEEE Electron Device Lett. **38**, 790 (2017).
[4]M. Hattori, T. Oshima, R. Wakabayashi, K. Yoshimatsu, K. Sasaki, T. Masui, A. Kuramata, S. Yamakoshi, K. Horiba, and H. Kumigashira, Jpn. J. Appl. Phys., Part 1 **55**, 1202B6 (2016).
[5]S. Rafique, L. Han, A. T. Neal, S. Mou, M. J. Tadjer, R. H. French, and H. Zhao, Appl. Phys. Lett. **109**, 132103 (2016).
[6]W. Y. Weng, T. J. Hsueh, and S. J. Chang, IEEE Sens. J. **11**, 1795 (2011).
[7]Y. W. Zhang, A. Neal, Z. Xia, C. Joishi, J. M. Johnson, Y. Zheng, S. Bajaj, M. Brenner, D. Dorsey, K. Chabak, G. Jessen, J. Hwang, S. Mou, J. P. Herenamns, and S. Rajan, Appl. Phys. Lett. **112**, 173502 (2018).
[8]T. Oshima, Y. Kato, N. Kawano, A. Kuramata, S. Yamakoshi, S. Fujita, T. Oishi, and M. Kasu, Appl. Phys. Express **10**, 035701 (2017).
[9]S. Krishnamoorthy, Z. Xia, C. Joishi, Y. Zhang, J. Mcglone, J. Johnson, M. Brenner, A. R. Arehart, J. Hwang, S. Lodha, and S. Rajan, Appl. Phys. Lett. **111**, 023502 (2017).
[10]F. Zhang, K. Saito, T. Tanaka, and M. Nishio, Appl. Phys. Lett. **105**, 162107 (2014).
[11]R. Schmidtgrund, C. Kranert, H. Von Wenckstern, V. Zviagin, M. Lorenz, and M. Grundmann, J. Appl. Phys. **117**, 165307 (2015).
[12]A. Ratnaparkhe and W. R. L. Lambrecht, Appl. Phys. Lett. **110**, 132103 (2017).
[13]J. B. Varley, J. R. Weber, A. Janotti, and C. G. Van de Walle, Appl. Phys. Lett. **97**, 142106 (2010).
[14]X. F. Ma, Y. M. Zhang, L. P. Dong, and R. X. Jia, Results Phys. **7**, 1582 (2017).
[15]J. P. Perdew, K. Burke, and M. Ernzerhof, Phys. Rev. Lett. **77**, 3865 (1996).
[16]J. Heyd, G. E. Scuseria, and M. Ernzerhof, J. Chem. Phys. **124**, 219906 (2006).
[17]G. Kresse and J. Furthmüller, Phys. Rev. B **54**, 11169 (1996).
[18]S. W. Kaun, F. Wu, and J. S. Speck, J. Vac. Technol., A **33**, 041508 (2015).
[19]H. Ito, K. Kaneko, and S. Fujita, Jpn. J. Appl. Phys., Part 1 **51**, 100207 (2012).
[20]R. Schewski, G. Wagner, M. Baldini, D. Gogova, Z. Galazka, T. Schulz, T. Remmele, T. Markurt, H. von Wenckstern, M. Grundmann, O. Bierwagen, P. Vogt, and M. Albrecht, Appl. Phys. Express **8**, 011101 (2015).
[21]Y. Oshima, E. Ahmadi, S. C. Badescu, F. Wu, and J. S. Speck, Appl. Phys. Express **9**, 061102 (2016).
[22]C. Kranert, M. Jenderka, J. Lenzner, M. Lorenz, H. von Wenckstern, R. Schmidt-Grund, and M. Grundmann, J. Appl. Phys. **117**, 125703 (2015).
[23]R. D. Shannon, Acta Crystallogr., Sect. A: Cryst. Phys., Diffr., Theor. Gen. Crystallogr. **32**, 751 (1976).
[24]H. Shin, Y. Luo, P. Ganesh, J. Balachandran, J. T. Krogel, P. R. C. Kent, A. Benali, and O. Heinonen, Phys. Rev. Mater. **1**, 073603 (2017).
[25]J. Papierska, A. Ciechan, P. Bogusławski, M. Boshta, M. M. Gomaa, E. Chikoidze, Y. Dumont, A. Drabińska, H. Przybylińska, A. Gardias, J. Szczytko, A. Twardowski, M. Tokarczyk, G. Kowalski, B. Witkowski, K. Sawicki, W. Pacuski, M. Nawrocki, and J. Suffczyński, Phys. Rev. B **94**, 224414 (2016).
[26]Z. Lin, A. Orlov, R. M. Lambert, and M. C. Payne, J. Phys. Chem. B **109**, 20948 (2005).
[27]T. Biswas, P. Ravindra, E. Athresh, R. Ranjan, S. Avasthi, and M. Jain, J. Phys. Chem. C **121**, 24766 (2017).
[28]B. W. Krueger, C. S. Dandeneau, E. M. Nelson, S. T. Dunham, F. S. Ohuchi, and M. A. Olmstead, J. Am. Ceram. Soc. **99**, 2467 (2016).
[29]L. Binet and D. Gourier, J. Phys. Chem. Solids **59**, 1241 (1998).
[30]T. Onuma, S. Fujioka, T. Yamaguchi, M. Higashiwaki, K. Sasaki, T. Masui, and T. Honda, Appl. Phys. Lett. **103**, 041910 (2013).
[31]E. G. Víllora, T. Atou, T. Sekiguchi, T. Sugawara, M. Kikuchi, and T. Fukuda, Solid State Commun. **120**, 455 (2001).
[32]A. Mock, R. Korlacki, C. Briley, V. Darakchieva, B. Monemar, Y. Kumagai, K. Goto, M. Higashiwaki, and M. Schubert, Phys. Rev. B **96**, 245205 (2017).
[33]C. Janowitz, V. Scherer, M. Mohamed, A. Krapf, H. Dwelk, R. Manzke, Z. Galazka, R. Uecker, K. Irmscher, and R. Fornari, New J. Phys. **13**, 085014 (2011).
[34]J. Lloyd-Hughes, M. Failla, J. D. Ye, K. L. Teo, and C. Jagadish, Appl. Phys. Lett. **106**, 202103 (2015).
[35]F. Xian, J. Ye, S. Gu, H. H. Tan, and C. Jagadish, Appl. Phys. Lett. **109**, 023109 (2016).
[36]E. A. Davis and N. F. Mott, Philos. Mag. A **22**, 0903 (1970).
[37]S. Canulescu, N. C. Jones, C. N. Borca, C. Piamonteze, K. Rechendorff, V. C. Gudla, K. Bordo, L. P. Nielsen, S. V. Hoffmann, and K. P. Almtoft, Appl. Phys. Lett. **109**, 091902 (2016).
[38]A. S. Pratiyush, S. Krishnamoorthy, S. V. Solanke, Z. Xia, R. Muralidharan, S. Rajan, and D. N. Nath, Appl. Phys. Lett. **110**, 221107 (2017).
[39]P. Feng, J. Y. Zhang, Q. H. Li, and T. H. Wang, Appl. Phys. Lett. **88**, 153107 (2006).